Comparison of outflow boundary conditions for subsonic aeroacoustic simulations

A. Fosso P.*, H. Deniau, N. Lamarque and T. Poinsot

CERFACS, CFD Team,
Av. G. Coriolis, 31057 Toulouse Cedex France

SUMMARY

Aeroacoustics simulations require much more precise boundary conditions than classical aerodynamics. Two classes of non-reflecting boundary conditions for aeroacoustics are compared in the present work: characteristic analysis based methods and Tam and Dong approach. In characteristic methods, waves are identified and manipulated at the boundaries while Tam and Dong use modified linearized Euler equations in a buffer zone near outlets to mimic a non-reflecting boundary. The principles of both approaches are recalled and recent characteristic methods incorporating the treatment of transverse terms are discussed. Three characteristic techniques (the original NSCBC formulation of Poinsot and Lele and two versions of the modified method of Yoo and Im) are compared to the Tam and Dong method for four typical aeroacoustics problems: vortex convection on a uniform flow, vortex convection on a shear flow, acoustic propagation from a monopole and from a dipole. Results demonstrate that the Tam and Dong method generally provides the best results and is a serious alternative solution to characteristic methods even though its implementation might require more care than usual NSCBC approaches.

KEY WORDS: Outflow conditions; characteristic boundary conditions; radiation boundary conditions

1. INTRODUCTION

Computational Aeroacoustics (CAA) methods must satisfy stringent constraints because of the wide range of scales and frequencies in the target flows. To deal with those requirements, high-order, low dispersion and low dissipation schemes are needed (1; 2). However, these schemes are also more sensitive to spurious waves generated by numerical boundary conditions. These high frequency waves can propagate in the domain and modify the acoustic field even if their effect on the aerodynamic field is small. Therefore, the development of accurate numerical boundaries is more difficult for aeroacoustics applications than for aerodynamics applications.

Most methods for boundary conditions in compressible flows are based on the expression of the hyperbolic part of the Navier-Stokes equations in characteristic form. Thompson (3) proposed a first boundary condition formulation for the Euler equations. Poinsot and Lele (4)

*Correspondence to: Hugues Deniau, deniau@cerfacs.fr

extended these characteristic methods to the Navier-Stokes equations, assuming that the flow is one-dimensional in the normal direction of the boundary: the so-called Local One Dimensional Inviscid (LODI) equations. They have then been improved to handle strongly multidimensional flows and aeroacoustics problems (5; 6; 7; 8; 9; 10) and all resulting methods are used for aeroacoustics problems. Another method commonly used is the Perfect Matched Layer (PML) method (11; 12; 13). This method gives good results when solving Linearized Euler Equations but is more difficult to apply on the general Navier-Stokes equations. A third method, which is specific to aeroacoustics problems, is the radiative and outflow conditions developed by Tam and coworkers (14; 15).

This study focuses on characteristic-based and the Tam and coworkers approaches. The two classes of methods are very different: (i) characteristic methods are based on a planar waves decomposition of the flow, whereas the Tam approach assumes that the acoustic waves are spheric and the vorticity and entropy waves are convected by a constant mean flow, (ii) the LODI methods are applied only on the outlet boundary, while the Tam conditions are generally imposed on a small layer near the outlet. The objective of this paper is to compare the two methodologies. This has already been done for pure acoustic test problems (16; 17; 18) but no recent work has addressed comparisons between recent characteristic-based methods and the Tam and coworkers approach in the same code and on a representative set of test problems for aeroacoustics applications. This study points out the advantages and drawbacks of each method by comparing them on a series of test problems: vortex convection through a non-reflective subsonic outlet, acoustic propagation from a monopole or a dipole.

The paper is organised as follows: section 3 presents the LODI approach and some improvements done to generalize it to a multi-dimensional outflow. Section 4 presents the conditions developed by Tam and coworkers. Section 5 describes comparisons between the different outflow conditions.

2. DISCRETIZATION OF THE COMPRESSIBLE NAVIER-STOKES EQUATIONS

2.1. Navier-Stokes equations

The compressible Navier-Stokes equations are (in conservative form):

$$\begin{aligned} \frac{\partial W}{\partial t} \quad &+\frac{\partial E_c}{\partial x}+\frac{\partial F_c}{\partial y}+\frac{\partial G_c}{\partial z} \\ &+\frac{\partial E_d}{\partial x}+\frac{\partial F_d}{\partial y}+\frac{\partial G_d}{\partial z} \quad = 0, \end{aligned} \tag{1}$$

where

$$W = (\rho, \rho u, \rho v, \rho w, \rho e)^t, \tag{2}$$

$$\begin{aligned} E_c &= \left(\rho u, \rho u^2 + p, \rho uv, \rho uw, (\rho e + p)u\right)^t, \\ F_c &= \left(\rho v, \rho uv, \rho v^2 + p, \rho vw, (\rho e + p)v\right)^t, \\ G_c &= \left(\rho w, \rho uw, \rho vw, \rho w^2 + p, (\rho e + p)w\right)^t, \end{aligned}$$

$$
\begin{aligned}
E_d &= (0, -\tau_{11}, -\tau_{12}, -\tau_{13}, -(\tau_{11}u + \tau_{12}v + \tau_{13}w) + q_1)^t, \\
F_d &= (0, -\tau_{21}, -\tau_{22}, -\tau_{23}, -(\tau_{21}u + \tau_{22}v + \tau_{23}w) + q_2)^t, \\
G_d &= (0, -\tau_{31}, -\tau_{32}, -\tau_{33}, -(\tau_{31}u + \tau_{32}v + \tau_{33}w) + q_3)^t,
\end{aligned}
$$

p is the pressure, τ the stress tensor and q the heat flux vector.

2.2. Finite-Volume discretization

Considering a volume Ω, the Finite-Volume discretization of Eq. (1) could be written:

$$
V\frac{\mathrm{d}\bar{W}}{\mathrm{d}t} + \sum_{m=1}^{N_f}\left(\tilde{\mathcal{F}}_c^m + \tilde{\mathcal{F}}_d^m\right) = 0, \tag{3}
$$

where $V = |\Omega|$, $\bar{W}$ is the averaged value of the field W over the cell Ω, N_f is the number of faces of the volume Ω,

$$
\tilde{\mathcal{F}}_c^m = \int_{\partial\Omega_m} (E_c n_x + F_c n_y + G_c n_z)\,\mathrm{d}S, \tag{4}
$$

and

$$
\tilde{\mathcal{F}}_d^m = \int_{\partial\Omega_m} (E_d n_x + F_d n_y + G_d n_z)\,\mathrm{d}S \tag{5}
$$

are the convective and diffusive fluxes through the $m-th$ face of Ω. The residual over the volume Ω is defined by:

$$
R_\Omega = \frac{1}{V}\sum_{m=1}^{N_f}\left(\tilde{\mathcal{F}}_c^m + \tilde{\mathcal{F}}_d^m\right). \tag{6}
$$

The numerical scheme is then defined by:

$$
\frac{\mathrm{d}\bar{W}}{\mathrm{d}t} = -R_\Omega, \tag{7}
$$

where R_Ω is computed, in general, using Eq. (6).

In the present paper, a cell-centered approach is used on structured meshes. Volumes correspond to the mesh cells and their faces are interfaces between neighbouring cells. For convective fluxes, the following approximation is used:

$$
\tilde{\mathcal{F}}_c^f \approx S(E_c(\tilde{W}_f)\tilde{n}_x^f + F_c(\tilde{W}_f)\tilde{n}_y^f + G_c(\tilde{W}_f)\tilde{n}_z^f). \tag{8}
$$

where $\tilde{\mathcal{F}}_c$ is the convective flux through the interface f considered, $\tilde{W}_f$ stands for the interface-averaged values of the conservative variables, which is computed using a compact interpolation scheme (19). The formulation of Eq. (8) is formally only second-order accurate, but it has been observed (19) that it could reach the fifth-order accuracy if the grid is sufficiently regular. For diffusive fluxes, a traditional second-order method (20) has been used. A sixth-order compact filtering operator of Visbal and Gaitonde (21) is used to eliminate odd-even oscillations.

3. NAVIER-STOKES CHARACTERISTIC BOUNDARY CONDITIONS (NSCBC)

3.1. Standard NSCBC

NSCBC are based on the expression of Euler equations in a characteristic form (3). Let us consider the 1D Euler equation:

$$\frac{\partial W}{\partial t} + \frac{\partial E_c}{\partial x} = 0. \tag{9}$$

Using a 1D characteristic analysis following the x-direction:

$$\mathfrak{D} = \frac{\partial E_c}{\partial x} = \begin{pmatrix} d_1 \\ ud_1 + \rho d_2 \\ vd_1 + \rho d_3 \\ wd_1 + \rho d_4 \\ \frac{1}{2}(u^2+v^2+w^2)d_1 + \rho u d_2 + \rho v d_3 + \rho w d_4 + \frac{1}{\gamma-1} d_5 \end{pmatrix}, \tag{10}$$

with

$$d = \begin{pmatrix} d_1 \\ d_2 \\ d_3 \\ d_4 \\ d_5 \end{pmatrix} = \begin{pmatrix} \mathcal{L}_1 + \frac{\rho}{2c}(\mathcal{L}_4 + \mathcal{L}_5) \\ \frac{1}{2}(\mathcal{L}_4 - \mathcal{L}_5) \\ \mathcal{L}_2 \\ \mathcal{L}_3 \\ \frac{\rho c}{2}(\mathcal{L}_4 + \mathcal{L}_5) \end{pmatrix}, \tag{11}$$

and

$$\mathcal{L} = \begin{pmatrix} u\left[\frac{\partial \rho}{\partial x} - \frac{1}{c^2}\frac{\partial p}{\partial x}\right] \\ u\left[\frac{\partial v}{\partial x}\right] \\ u\left[\frac{\partial w}{\partial x}\right] \\ (u+c)\left[\frac{\partial u}{\partial x} + \frac{1}{\rho c}\frac{\partial p}{\partial x}\right] \\ (u-c)\left[-\frac{\partial u}{\partial x} + \frac{1}{\rho c}\frac{\partial p}{\partial x}\right] \end{pmatrix}. \tag{12}$$

$\mathcal{L}$ is the vector of characteristic wave amplitudes. Following the sign of the eigenvalues (u,$u+c$ and $u-c$), the characteristic waves are distinguished as incoming or outgoing waves. Outgoing waves are computed using interior points and one-sided schemes, while the incoming waves must be evaluated using information on the boundary condition and Eq. (9). Standard LODI method (4) assumes that the flow crossing the boundary is almost inviscid and one-dimensional along the normal direction of the boundary interface (which will correspond to the x-axis), so that the term $\mathfrak{D}$ can be computed using characteristic wave amplitudes. In addition, the other terms of the Navier-Stokes equations (transverse convective fluxes and viscous fluxes in Eq. (1)) are computed as usually and taken into account separately.

For a subsonic outflow condition at the boundary $x = x_{\max}$, only the eigenvalue $u - c$ is negative. Therefore, except from $\mathcal{L}_5$, all characteristic wave amplitudes can be computed using an upwind scheme. To obtain $\mathcal{L}_5$, the boundary condition and a LODI equation must be used. If the outlet pressure is imposed and constant, the LODI condition (3) provides the following value of $\mathcal{L}_5$:

$$\mathcal{L}_5 = -\mathcal{L}_4. \tag{13}$$

This outflow condition is completely reflective and is not used in general for aeroacoustics. A non-reflective outflow condition can be obtained by cancelling out the incoming waves, thus by setting

$$\mathcal{L}_5 = 0. \tag{14}$$

However, this latter condition can lead to a drifting mean pressure, because the boundary condition has no indication of the target pressure to reach. Poinsot and Lele (4) recommend to set:

$$\mathcal{L}_5 = K(p - p_{\text{tar}}), \tag{15}$$

with p_{tar} the target pressure. For example, in a non viscous 1D case, the relaxation coefficient K is defined so that the final outflow condition matches the partially non-reflecting outflow condition of Rudy and Strickwerda (22):

$$\frac{\partial p}{\partial t} - \rho c \frac{\partial u}{\partial t} = -\sigma c \frac{1 - \mathcal{M}_{\max}^2}{L}(p - p_{\text{tar}}), \tag{16}$$

where L is a reference length, $\mathcal{M}_{\max}$ is the maximum mach number on the boundary, c is the sound speed and σ is a parameter, which is generally set to 0.25.

3.2. Modified outflow characteristic-based conditions

Some authors (7; 8; 10) have improved the standard NSCBC method by accounting differently for the contribution of transverse derivatives and viscous fluxes. Indeed, the complete Navier-Stokes equations, using characteristic variables, can be written

$$\begin{bmatrix} c^2\frac{\partial \rho}{\partial t} - \frac{\partial p}{\partial t} \\ \frac{\partial v}{\partial t} \\ \frac{\partial w}{\partial t} \\ \frac{\partial p}{\partial t} + \rho c \frac{\partial u}{\partial t} \\ \frac{\partial p}{\partial t} - \rho c \frac{\partial u}{\partial t} \end{bmatrix} + \begin{bmatrix} c^2\mathcal{L}_1 \\ \mathcal{L}_2 \\ \mathcal{L}_3 \\ \rho c \mathcal{L}_4 \\ \rho c \mathcal{L}_5 \end{bmatrix} + \begin{bmatrix} \mathcal{T}_1 \\ \mathcal{T}_2 \\ \mathcal{T}_3 \\ \mathcal{T}_4 \\ \mathcal{T}_5 \end{bmatrix} + \begin{bmatrix} \mathcal{D}_1 \\ \mathcal{D}_2 \\ \mathcal{D}_3 \\ \mathcal{D}_4 \\ \mathcal{D}_5 \end{bmatrix} = \begin{bmatrix} 0 \\ 0 \\ 0 \\ 0 \\ 0 \end{bmatrix}, \tag{17}$$

where $\mathcal{T}$ contains all transverse terms and $\mathcal{D}$ are the diffusive terms. Yoo and Im (7) proposed to take into account only a part β of $\mathcal{T}_5$ and $\mathcal{D}_5$ so that the final non-reflecting boundary condition can be written:

$$\left(\frac{\partial p}{\partial t} - \rho c \frac{\partial u}{\partial t}\right) + K(p - p_{\text{tar}}) + \beta(\mathcal{T}_5 + \mathcal{D}_5) = 0, \tag{18}$$

by setting $\mathcal{L}_5$ to:

$$\mathcal{L}_5 = K(p - p_{\text{tar}}) + (\beta - 1)(\mathcal{T}_5 + \mathcal{D}_5), \tag{19}$$

with $K = \sigma c \frac{1-\mathcal{M}_{max}^2}{L}$ and $\beta \in [0, 1]$. Yoo and Im (7) show, using a low Mach number analysis, that the parameter β must scale like the reference Mach number. However, the definition of this parameter is still an issue for inhomogeneous flows. Lodato *et al* (8) and Granet *et al* (23) compare values of β based on the mean value of the Mach number on the outlet or on its local value. They conclude that it is more efficient to use the mean Mach number on the boundary. Liu and Vasilyev (10), through three-dimensional characteristic decomposition of the Euler equations, propose a formulation in which the weighting coefficient β is applied on certain

transverse terms only. They show that β depends on the flow and on the wave angle crossing the boundary. Lastly, Prosser(6) derived another improvement of the LODI method by using a scales separation on the problem of vortex convection. Nevertheless this separation remains difficult to perform for general flows. The next section describes the characteristic approaches retained here.

3.3. Implementation of characteristic methods

In this work, three characteristic-based methods have been retained: the standard LODI method, the method of Yoo and Im (7) using the local Mach number as the parameter β and this same method but using a given reference Mach number for β. The boundary conditions are applied not at the boundary interfaces but at the boundary cell centers. Hence, fluxes are not computed using Eq. (8) but are modified such that the residual defined in Eq. (6) is equal to the one given by the characteristic-based approach. Therefore, the final residual is given by

$$\begin{aligned} R_{\Omega_b} &= \mathfrak{D} + \frac{\partial F_c}{\partial y} + \frac{\partial G_c}{\partial z} \\ &\quad + \frac{\partial E_d}{\partial x} + \frac{\partial F_d}{\partial y} + \frac{\partial G_d}{\partial z}, \end{aligned} \tag{20}$$

where Ω_b is a boundary cell, $\mathfrak{D}$ is given by Eq. (10). For the standard LODI approach, $\mathcal{L}_5$ is defined by Eq. (15), while it is defined by Eq. (19) for the methods of Yoo and Im with β as the local Mach or a reference Mach number. For all test cases, no relaxation term is applied ($K = 0$).
Outgoing characteristic waves are computed using second-order one-sided FD scheme. The flux balance following the transverse grid directions is used to approximate the transverse derivatives. When the mesh is not cartesian, metric terms have to be computed but the issues of curvilinear grids are not addressed in this paper.

4. TAM AND DONG OUTFLOW BOUNDARY CONDITION

An alternative method to characteristic techniques, initially proposed by Tam and Webb (14), is to sacrifice a part of a domain and solve a different set of equations in this zone. This new set of equations is modified to minimize acoustic reflections. It is assumed that all acoustic waves spherically radiate from a single point in a uniform mean flow. This allows to minimize reflections and provides pure radiation. The outflow boundary condition of Tam and Dong (15) generalizes this radiation boundary condition of Tam and Webb (14) to weakly non-uniform mean flows. The condition is based on linearized Euler equations.

4.1. Outflow equations

This condition is based on three main assumptions:

1. the mean flow is weakly non-homogeneous;
2. pressure fluctuations are only acoustic;
3. acoustic waves are propagating in the far field (obstacle-free) following the radial direction relative to the single noise source;

4. vorticity or entropy waves are convected at the mean flow speed.

Tam and Dong (15) derived outflow equations for 2D problems using these assumptions. Bogey and Bailly (24) extended them to 3D cases.
In spherical coordinates (r, θ, ϕ) (Fig. 1) with origin at the noise source, and basis vectors $(\vec{e_r}, \vec{e_\theta}, \vec{e_\phi})$ defined as:

$$\begin{cases} \vec{e_r} = (\sin\theta\cos\phi\,,\ \sin\theta\sin\phi\,,\ \cos\theta) \\ \vec{e_\theta} = (\cos\theta\cos\phi\,,\ \cos\theta\sin\phi\,,\ -\sin\theta) \\ \vec{e_\phi} = (-\sin\phi\,,\ \cos\phi\,,\ 0) \end{cases}, \tag{21}$$

the system of equations to apply on the outflow layer is given by

$$\begin{aligned} \frac{\partial(\rho-\bar\rho)}{\partial t} + \overrightarrow{V}\cdot\overrightarrow{\nabla}(\rho-\bar\rho) &= \frac{1}{\bar a^2}\frac{\partial p_a}{\partial t} + \overrightarrow{V}\cdot\overrightarrow{\nabla}\left(\frac{p_a}{\bar a^2}\right) \\ \frac{\partial(u-\bar u)}{\partial t} + \overrightarrow{V}\cdot\overrightarrow{\nabla}(u-\bar u) &= -\frac{1}{\bar\rho}\frac{\partial p_a}{\partial x} \\ \frac{\partial(v-\bar v)}{\partial t} + \overrightarrow{V}\cdot\overrightarrow{\nabla}(v-\bar v) &= -\frac{1}{\bar\rho}\frac{\partial p_a}{\partial y} \\ \frac{\partial(w-\bar w).}{\partial t} + \overrightarrow{V}\cdot\overrightarrow{\nabla}(w-\bar w) &= -\frac{1}{\bar\rho}\frac{\partial p_a}{\partial z} \\ \frac{1}{V_g}\frac{\partial p_a}{\partial t} + \frac{\partial p_a}{\partial r} + \frac{1}{\alpha r}(p_a) &= 0 \end{aligned} \tag{22}$$

with $\alpha = 2$ in 2D or 1 in 3D, and

$$p = \bar p + p_a,$$

where $\bar\rho$, $\overrightarrow{V} = (\bar u, \bar v, \bar w)$, $\bar p$, $\bar a$ are the mean flow density, velocity, pressure and sound speed and p_a is the acoustic pressure fluctuation. V_g is the group velocity of acoustic waves (see Fig. 2) defined by:

$$V_g = \overrightarrow{V}\cdot\vec{e_r} + \sqrt{\bar a^2 - (\overrightarrow{V}\cdot\vec{e_\theta})^2 - (\overrightarrow{V}\cdot\vec{e_\phi})^2} \tag{23}$$

and

$$\frac{\partial}{\partial r} = \vec{e_r}\cdot\overrightarrow{\nabla} = \sin\theta\cos\phi\frac{\partial}{\partial x} + \sin\theta\sin\phi\frac{\partial}{\partial y} + \cos\theta\frac{\partial}{\partial z}.$$

Since the mean flow speed is supposed to be constant in time, the Tam and Dong outflow system could read as:

$$\begin{aligned} \frac{\partial\rho}{\partial t} + \overrightarrow{V}\cdot\overrightarrow{\nabla}(\rho-\bar\rho) &= \frac{1}{\bar a^2}\frac{\partial p}{\partial t} + \overrightarrow{V}\cdot\overrightarrow{\nabla}\left(\frac{p-\bar p}{\bar a^2}\right) \\ \frac{\partial u}{\partial t} + \overrightarrow{V}\cdot\overrightarrow{\nabla}(u-\bar u) &= -\frac{1}{\bar\rho}\frac{\partial(p-\bar p)}{\partial x} \\ \frac{\partial v}{\partial t} + \overrightarrow{V}\cdot\overrightarrow{\nabla}(v-\bar v) &= -\frac{1}{\bar\rho}\frac{\partial(p-\bar p)}{\partial y} \\ \frac{\partial w}{\partial t} + \overrightarrow{V}\cdot\overrightarrow{\nabla}(w-\bar w) &= -\frac{1}{\bar\rho}\frac{\partial(p-\bar p)}{\partial z} \\ \frac{1}{V_g}\frac{\partial(p-\bar p)}{\partial t} + \frac{\partial(p-\bar p)}{\partial r} + \frac{1}{\alpha r}((p-\bar p)) &= 0 \end{aligned} \tag{24}$$

The implementation of this outflow condition also raises the problem of the definition of the mean flow. In the test case used by Tam and Dong (15), the mean flow is an analytical asymptotic solution of the problem. This type of solution is not always available for general flows.

Another important drawback of this condition is to fail to take into account pressure fluctuations due to vorticity waves. Indeed, Bogey and Bailly (24) point out the fact that at the end of the domain, a sponge layer zone is generally used in order to damp the vorticity fluctuations out before they reach the outlet. This sponge layer can significantly reduce reflections.

4.2. Implementation of Tam and Dong outflow condition

The Tam and Dong outflow condition is applied on a outflow layer rather than on the outflow boundary only (Fig. 3). This allows a smooth and silent transition from the N.-S. equations to the outflow equations. In this outflow layer, the residual of Eq. (7) is computed using Eq. (24). The spatial derivatives are computed using second-order FD schemes. These second-order FD schemes are centered when possible and one-sided otherwise.

The next section presents comparisons between the characteristic-based and the Tam and Dong outflow boundary conditions.

5. COMPARISONS OF OUTFLOW CONDITIONS

In this section, different flow cases are tested using four outflow boundary conditions (Tab. I) are:

- the non-reflective subsonic outlet condition defined using the standard LODI method of Poinsot and Lele (4) without any relaxation on the pressure field (OC1);
- the non-reflective subsonic outlet condition using the characteristic-based method of Yoo and Im (7) using the local Mach number to compute the contribution of the transverse and viscous terms (OC2);
- the non-reflective subsonic outlet condition using the characteristic-based method of Yoo and Im (7) using a reference Mach number to compute the contribution of the transverse and viscous terms (OC3);
- the outflow condition of Tam and Dong (15) (OC4) using three points in the outflow layer.

Code	Boundary condition
OC1	Outflow condition of Poinsot and Lele (4)
OC2	Outflow condition of Yoo and Im (7) using the local mach number
OC3	Outflow condition of Yoo and Im (7) using a reference mach number
OC4	Outflow condition of Tam and Dong (15)

Table I. Boundary conditions compared

Test cases are listed in Tab. II. The first test problems (VCUF and VCSF) are vortices crossing outlet boundaries. While VCUF corresponds to a usual test problem for boundary conditions (a vortex crossing a boundary in a constant mean flow), VCSF introduces a more difficult configuration where the vortex is convected in a mean flow which is sheared so the local Mach number at the outlet is not constant. The other test problems (APM and APD) correspond to pure acoustic waves crossing boundaries. It is worth noting that test problems

	Name	Section	Objective
VCUF:	Vortex Convection in an Uniform Flow	Sect. 5.1.1	Same Test cases as (4) but in Euler Configuration
VCSF:	Vortex Convection in a linearly Shear Flow	Sect. 5.1.2	Effect of the mean velocity gradient on boundaries
APM:	Acoustic Propagation from monopole	Sect. 5.2.1	Acoustic waves crossing boundaries
APD:	Acoustic Propagation from a dipole	Sect.5.2.2	Reflected acoustic waves crossing boundaries

Table II. Test problems realized

VCUF and VCSF using the different characteristic-based approaches were repeated using a completely different solver (AVBP (25)) and gave the same results. This confirms the correct implementation of the boundary conditions and shows that the present conclusions do not depend on the numerical solver used in the domain.

5.1. Vortex convection

5.1.1. Vortex convection in an uniform flow (VCUF) This test consists in convecting a Lamb-Oseen vortex in the x-direction. The initial vortex is given by the stream function:

$$\Psi(x,y) = \Gamma \exp\left(-\frac{x^2+y^2}{2R^2}\right), \tag{25}$$

where Γ is the vortex strength and R the vortex radius. The resulting velocity distribution is obtained through the velocity stream function relationship:

$$u = U_\infty - \frac{\partial \Psi}{\partial y},\ v = \frac{\partial \Psi}{\partial x}. \tag{26}$$

The associated pressure variation follows the radial momentum equation:

$$p - p_\infty = -\frac{\rho \Gamma^2}{2R^2} \exp\left(-\frac{x^2+y^2}{R^2}\right). \tag{27}$$

The maximum speed induced by the vortex in the x-direction is given by:

$$U_{\text{vort}} = \frac{\Gamma}{R\sqrt{e}}. \tag{28}$$

The computational domain which is $2L$ long in x and y directions, is discretized using a 65×65 nodes uniform cartesian mesh. The inflow is defined using a standard LODI method. The boundaries in the y-direction are periodic boundaries.

Case	U_∞^+	U_{vort}/U_∞
A	0.5	0.75
B	0.05	0.75
C	0.5	0.25
D	0.05	0.25

Table III. Test cases of vortex convection in an uniform flow

Vortices are initialized in the center of the domain and leave it at a time L/U_∞ corresponding to a reduced time:

$$t^+ = \frac{L}{U_\infty}\frac{c}{L} = \frac{1}{M}.$$

Velocities are normalized by the sound speed and the normalized pressure is defined by:

$$p^* = \frac{p - p_\infty}{|p(0,0) - p_\infty|}. \tag{29}$$

Four different cases are considered (Tab. III). For each case, the reference Mach number used for OC3 corresponds to the mean Mach number of the case. The source point for OC4 is set to the center of the inlet, *i.e.* at $(-1, 0)$. Several tests show that it is sufficient to put it far upstream of the outlet and that results depend weakly on its position.

Case A VCUF: 0.5 Mach flow and strong vortex Fig. 4 shows isocontours of the streamwise flow speed u^+ and grey scales of the pressure field at times $t^+ = 0$, 2 and 3 for case A. Fig. 5 shows the profiles of u^+ and p^* along the line $x = 0.9$ and at times $t^+ = 2.0$ and $t^+ = 3.0$ and Fig. 12(a) displays the time-evolution of $p^*_{\max} - p^*_{\min}$, which allows to evaluate the pressure wave reflections when the vortex leaves the domain.
With OC1, the pressure range strongly increases and the pressure field is no more symmetric with respect to the y-axis. When the vortex is supposed to be entirely out of the domain, the velocity field deviates from the exact solution. On the other hand, OC2, OC3 and OC4 give results in good agreement with the exact solution. At time $t^+ = 3$, the reflected pressure waves generated by OC2 and OC3 methods are more important than the ones generated by OC4 method. This is true at least until $t^+ = 8$ as shown by Fig. 12(a).

Case B VCUF: 0.05 Mach flow and strong vortex The isocontours of the streamwise velocity u^+ and the grey scales of the normalized pressure p^* field at times $t^+ = 0$, 20, 30 are shown in Fig. 6. Fig. 7 shows the profiles of u^+ and p^* along the line $x = 0.9$ at times $t^+ = 20$, 30 and Fig. 12(b) shows the evolution of $p^*_{\max} - p^*_{\min}$ versus the time.
This case seems more difficult since for all methods, spurious waves are more visible on pressure greyscales than for case A. The standard LODI method (OC1) still gives poor results for the pressure field, even worse than for the case A. Surprisingly, the streamwise velocity for OC1 is always in good agreement with the exact solution. Fig. 7 shows that, at time $t^+ = 20$, the pressure profile obtained with the characteristic-based method OC2 is underestimated. In fact, the pressure field is shifted down compared to the exact solution. This is why the scale used for the pressure greyscales has been shifted. At $t^+ = 30$, the underestimation is no longer present but the velocity field is still oscillating showing that the condition is not completely reflecting.

Meanwhile, results for OC3 are in very good agreement with exact solution both for pressure and velocity field.
OC4 correctly performs at $t^+ = 20$ but finally overestimates the pressure field when the vortex is supposed to be completely out of the domain at time $t^+ = 30$. This induces the reflected wave observed on the velocity profile in Fig. 7 (a sign change of the velocity is observed at $t^+ = 30$), since the pressure gradient is a source term in the momentum equations (see Eq. (24)). Therefore, for this case, contrary to case A, OC3 performs better than OC4 during all the simulation.

Case C VCUF: 0.5 Mach flow and weak vortex Results are qualitatively similar to those obtained in case A. Indeed, as shown by u^+ isocontours and grey scales of the p^* field at times $t^+ = 0$, 2, 3 in Fig. 8 or profiles of p^* and u^+ along the line $x = 0.9$ in Fig. 9, OC1 still gives poor results on pressure and on velocity. At $t^+ = 2$, the pressure field is completely different from the exact solution. When the vortex is supposed to be out of the domain at $t^+ = 3$, high amplitude oscillations are still present on both pressure and velocity fields. Whereas, other methods correctly perform and OC4 generates less reflections than all the others when the vortex has completely left the domain as shown also by the time-evolution of $p^*_{\max} - p^*_{\min}$ in Fig. 12(c). It can thus be concluded that when the Mach number is high, independently to the vortex strength, OC4 correctly performs and better than characteristic-based methods considered.

Case D: 0.05 Mach flow and weak vortex Case D gives also results qualitatively similar to those obtaines in case B (same Mach flow). Fig. 10 shows grey scales of the normalized pressure with isocontours of the streamwise velocity, Fig. 11 shows profiles along the line $x = 0.9$ of p^* and u^+ at times $t^+ = 20$, 30 and Fig. 11 presents the time evolution of $p^*_{\max} - p^*_{\min}$. It could be observed that OC1 gives erroneous results on pressure but quite good ones on the velocity field. OC2 underestimates the pressure field at time $t^+ = 20$ but this deviation is no more visible at $t^+ = 30$. OC4 overestimates the pressure at $t^+ = 30$ and generates spurious waves on the velocity. Globally, OC3 correctly performs although some oscillations on the velocity profile at $t^+ = 30$ can be observed.
Therefore, it is clear that the behaviour of the differents methods is not much dependent of the vortex strength, provided the vortex velocity is less than the mean flow speed. OC3 correctly performs for each case, but OC4 generates less reflection when the Mach number is sufficiently high.

5.1.2. Vortex convection in a shear flow (VCSF) This test problem differs from the previous by the definition of the base flow. For VCSF, the base flow is a linear shear flow in the y-direction with $u_b = u_b(y)$ where $u_b(-1) = 0$ and $u_b(1) = U_{\max}$. Thus, the velocity is given by

$$u = u_b(y) - \frac{\partial \Psi}{\partial y},\ v = \frac{\partial \Psi}{\partial x}. \tag{30}$$

where $y = -1$ and $y = 1$ boundaries are slip walls. As for the previous VCUF test problem, different Mach number flows are simulated. However, since results for VCUF depend weakly on the vortex intensity, only the vortex whose speed is 75% of the maximum flow speed is considered (Tab. IV). For each case, the reference Mach number for the OC3 method is

Case	$U_{\max}$	$U_{\text{vort}}/U_{\max}$
A	0.5	0.75
B	0.05	0.75

Table IV. Test cases of vortex convection in a shear flow (VCSF).

$U_{\max}/2$. The source point for OC4 is also set at the center of the inlet.

Since no exact solution is known for the present problem, the same computations have been done on the domain :$-1 \leq y \leq 1$ and $-3 \leq x \leq 5$, with a double resolution. The solution over the domain of interest $-1 \leq x, y \leq 1$ is then extracted and referred to as a reference solution (REFSOL in figures). During the simulation time considered, the inlet and the outlet on this larger domain are supposed to have minor influence on this reference solution: indeed, considering a Mach of 0.5 for example, the reduced time needed for perturbations to propagate and reflect on the inlet at $x = -3$ or the outlet at $x = 5$ is of the order of 6 so that only time smaller than $t^+ = 6$ is considered for comparison.

Case A (VCSF): for a Mach of 0.5 Fig. 13 shows the normalized pressure p^* grey scales and streamwise velocity u^+ isocontours at times $t^+ = 2$, 4 and 6. Fig. 14 shows profiles of p^* and u at times $t^+ = 2$, 4, 6. OC1 still gives poor results on the pressure and velocity fields. The other methods are in good agreement with the reference solution with OC3 having the best behaviour. Indeed, OC2 and OC4 slightly underestimate the pressure at $t^+ = 6$, when the vortex is almost completely out of the domain.

Case B (VCSF): for a Mach of 0.05 Considering normalized pressure grey scales and streamwise velocity isocontours (Fig. 15), at time $t^+ = 20.0$, computations with OC1 seem satisfying but the pressure profiles at $x = 0.9$ (Fig. 16) are already very different from the reference solution. This goes worse at further times. OC2 and OC3 behave simirlaly at least until $t^+ = 40.0$. The pressure profiles at $x = 0.9$ at times $t^+ = 20$, 40 (Fig. 16) show that the computations lead to a surpression in low speed flow zone and a depression in high speed flow zone at the outlet. This is clearly different from the reference results. There is a slight phase shift on the velocity profiles (Fig. 16) at $t^+ = 40$ for OC1, OC2 and OC3. Finally, at $t^+ = 60$, the pressure profiles shapes are similar to the one of the reference computations, but OC2 strongly underestimates the pressure field while OC3 slightly overestimates it. On the other hand, OC4 always keeps the right pressure profile shape near the outlet but generally under- or over-estimates the pressure levels. Indeed, at $t^+ = 40$, the pressure in the domain is much too high, since it ranges between -0.3 and 0.17 while it ranges between -0.74 and 0.06 in reference solutions. At $t^+ = 60$, the pressure is rather too low with ranges [-0.2,-0.16] in comparison with [-0.04,0.03] in the reference computations. However, in this case, the pressure drifting does not influence velocity profiles which are in good agreement with the reference computations.

These results do not allow to determine which of the different methods is the most satisfactory but rather highlight weaknesses of each. For OC2, OC3 and OC4 weakly shear flows are difficult to handle. However it is clear that OC3 generally behaves better than the other characteristic methods. For all test cases, the reference Mach number is equal to the

mean Mach number on the outlet. Therefore, these results confirm those obtained by Lodato *et al* (8) and Granet *et al* (23).

5.2. Acoustic propagation

Two cases are considered here. The first one is the acoustic propagation from a monopole and the second from a dipole.

5.2.1. Acoustic propagation from a monopole An initial acoustic pulse is placed at the point $(0, 0)$ and radiates in a medium at rest. The acoustic pulse is defined by:

$$p' = \epsilon \exp\left[-\frac{\ln 2}{25}\left(x^2 + y^2\right)\right], \tag{31}$$

with $\epsilon = 1\text{Pa}$ and $P_\infty = 1. \times 10^5\text{Pa}$.
Computations are done on the domain $-100 \leq x^+, y^+ \leq 100$ using an uniform mesh with $\Delta x^+ = 1$. The time step is $\Delta t^+ = 0.5$.

Four simulations are carried out using each outflow condition of Tab. I. Pressure isocontours at times $t^+ = 100$, 120 and 180 are presented in Fig. 17. At $t^+ = 100$, the acoustic wave is just beginning to interact with the outlets. All boundary conditions behave correctly. At $t^+ = 120$, distortions appear on results for OC1, OC2 and OC3. The distortion orientation for the standard LODI method OC1 is opposite to the one for the characteristic-based methods OC2 and OC3 and it is a clear consequence of the fact that transverse terms are accounted for differently. Indeed, in this case, OC1 takes into account the whole contribution of transverse terms while OC2 only takes a very unsignificant part and OC3 nothing. However, these wave perturbations are very small since they are not visible when comparing pressure profiles along the line $x^+ = 99.0$ to the exact solution (Fig. 18). At $t^+ = 180$, the acoustic wave must be completely out of the domain but it is clear that OC1, OC2 and OC3 generates more spurious waves in the domain than OC4. However OC4 generates a slight depression in the domain but it is negligible.

5.2.2. Acoustic propagation from a dipole (APD) This second acoustic test problem is the first problem of the fourth category of the first workshop ICASE-NASA (16). It consists in the reflection of an initially gaussian acoustic wave on a slip wall boundary. The mean flow speed corresponds to a Mach number of 0.5 in the x-direction. An acoustic pulse is initially placed at $(0, 25)$. Generated acoustic waves are convected by the mean flow and encounter a wall at $y^+ = 0$, on which they are reflected. The acoustic perturbations introduced are given by:

$$p' = \epsilon \exp\left[-\frac{\ln 2}{25}\left(x^2 + (y-25)^2\right)\right], \text{ with } \epsilon = 1\text{Pa}. \tag{32}$$

The far field pressure is $P_\infty = 1. \times 10^5\text{Pa}$. The computational domain is given by $-100 \leq x^+ \leq 100$ and $0 \leq y^+ \leq 200$. The mesh is uniform. As in the APM test problem, $\Delta x^+ = 1$ and $\Delta t^+ = 0.5$.

The inflow is specified using a LODI approach (4).

Pressure isocontours are presented in Fig. 19. The characteristic-based methods generate spurious waves visible through the distortion of the pressure contours near the $y = y_{\max}$ outlet. As for APM test problem, the distortion is oriented differently for OC2 and OC3 compared

with OC1. These distortions, which appear also on APM results, are probably due to the fact that spherical waves are considered as a planar wave through the one dimensional assumption of OC1, OC2 and OC3. Acoustic reflections become more important when acoustic waves reach the corner (see results at $t^+ = 180$ on Fig. 20). They appear to be more important for OC2 and OC3 than for OC1. This result could be improved by the procedure proposed by Lodato *et al*(8).

Fig. 20 shows profiles of the pressure along the line $x = 99$. The pressure extrema along the line are smaller for OC2 and OC3 than for OC1 and OC4. This could be explained by the fact that the part of the transverse fluxes taken into account acts on pressure as a relaxation term. Therefore, the pressure fluctuations on boundary are damped. In general, compared with characteristic-based methods and the exact solution, the Tam and Dong outflow condition performs very well.

6. CONCLUSION

This work has focused on with the issue of outflow boundary conditions for aerodynamic simulations done for aeroacoustic purposes. Four boundary conditions have been tested: three characteristic-based boundary conditions and the radiative outlet using the Tam and coworkers equations. The three characteristic-based methods are the standard LODI approach of Poinsot and Lele (4) and the modified LODI approaches proposed by Yoo and Im (7) using a local Mach number and a reference Mach number respectively. The implementation of these outflow conditions in a solver using a compact cell-centered Finite Volume scheme has been presented.

Comparisons have been done for cases of vortex convection (in an uniform flow and in a linearly shear flow) and of acoustic propagation (in a medium at rest or with an uniform flow, in presence or not of an obstacle). Although the implementation of characteristic-based approaches could be improved, the Tam and Dong outflow condition is the best approach for pure acoustic radiation problems. For vortex convection in an uniform flow with a low Mach number or in a shear flow with a high Mach number, the characteristic-based condition using a reference Mach number to weight transverse terms contribution is the best method. For weakly shear flow at low Mach number, all methods are to be improved. However, the Tam and Dong outflow condition behaves better for vortex convection if the Mach number is sufficiently high to avoid a long interaction of pure hydrodynamic pressure fluctuations with the outlet. Indeed, in this case, it generates less important reflected waves than all other methods.

REFERENCES

[1] Lele SK. Compact finite difference schemes with spectral-like resolution. *Journal of Computational Physics* 1992; **103**:16–42.

[2] Freund JB. Noise sources in a low-reynolds-number turbulent jet at mach 0.9. *Journal of Fluid Mechanics* 2001; **438**:277–305.

[3] Thompson KW. Time dependent boundary conditions for hyperbolic systems. *Journal of Computational Physics* 1987; **68**:1–24.

[4] Poinsot TJ, Lele SK. Boundary conditions for direct simulations of compressible viscous flows. *Journal of Computational Physics* Jul 1992; **101**:104–129.

[5] Giles MK. Non-reflecting boundary conditions for euler equations calculations. *AIAA Journal* 1990; **28**:2050–2058.

[6] Prosser R. Improved boundary conditions for the direct numerical simulation of turbulent subsonic flows. i: inviscid flows. *Journal of Computational Physics* 2005; **207**:736–768.

[7] Yoo CS, Im HG. Characteristic boundary conditions for simulations of compressible reacting flows with multi-dimensional, viscous and reaction effects. *Combustion Theory and Modelling* April 2007; **11**(2):259–286.

[8] Lodato G, Domingo P, Vervisch L. Three-dimensional boundary conditions for direct and large-eddy simulation of compressible viscous flows. *Journal of Computational Physics* 2008; **227**:5105–5143.

[9] Guézennec N, Poinsot T. Acoustically nonreflecting and reflecting boundary conditions for vorticity injection in compressible solvers. *AIAA Journal* 2009; **47**:1709–1722.

[10] Liu Q, Vasilyev OV. Nonreflecting boundary conditions based on nonlinear multidimensional characteristics. *International Journal for Numerical Methods in Fluids* 2010; **62**(1):24–55.

[11] Berenger JP. A perfectly matched layer for the absorption of electromagnetic waves. *Journal of Computational Physics* 1994; **114**:185–200.

[12] Tam CKW, Auriault L, Cambuli F. Perfectly matched layer as an absorbing boundary condition for the linearized euler equations in open and ducted domains. *Journal of Computational Physics* 1998; **144**:213–234.

[13] Hu FQ. A perfectly matched layer absorbing boundary condition for linearized euler equations with a non-uniform mean flow. *Journal of Computational Physics* 2005; **208**(2):469–492.

[14] Tam CKW, Webb JC. Dispersion-relation-preserving finite difference schemes for computational acoustics. *Journal of Computational Physics* August 1993; **107**(2):262–281.

[15] Tam CKW, Dong Z. Radiation and outflow boundary conditions for direct computation of acoustic and flow disturbances in a nonuniform mean flow. *Journal of Computational Acoustics* 1996; **4**(2):175–201.

[16] Hardin JC, Ristorcelli JR, Tam CKW ((eds.)). *ICASE/LaRC Workshop on Benchmark Problems in Computational Aeroacoustics (CAA)*, NASA and ICASE: Hampton, Virginia, 1994.

[17] Tam CKW, Hardin JC ((eds.)). *Second Computational Aeroacoustics (CAA) Workshop on Benchmark Problems*, NASA and the Florida State University: Tallahassee, Florida, 1996.

[18] Hixon R, Shih SH, Mankbadi RR. Evaluation of boundary conditions for computational aeroacoustics. *AIAA Journal* 1995; **33**:2006–2012.

[19] Fosso Pouangue A, Deniau H, Sicot F, Sagaut P. Curvilinear finite-volume schemes using high-order compact interpolation. *Journal of Computational Physics* 2010; **229**(13):5090–5122.

[20] Cambier L, Veuillot J. Status of the elsa software for flow simulation and multi-disciplinary applications. *46^{th} AIAA Aerospace Sciences Meeting and Exhibit*, AIAA Paper 2008-0664: Reno (USA), 2008.

[21] Visbal MR, Gaitonde DV. On the use of higher-order finite-difference schemes on curvilinear and deforming meshes. *Journal of Computational Physics* September 2002; **181**(1):155–185.

[22] Rudy D, Strikwerda J. A nonreflecting outflow boundary condition for subsonic navier-stokes calculations. *Journal of Computational Physics* 1980; **36**:55–70.

[23] Granet V, Vermorel O, Leonard T, Gicquel L, Poinsot T. Comparison of non-reflecting boundary conditions for compressible solvers at subsonic outlets in complex geometries. *AIAA Journal* 2010; **Submitted on dec. 18, 2009**.

[24] Bogey C, Bailly C. Three-dimensional non-reflective boundary conditions for acoustic simulations: far field formulation and validation test cases. *Acta Acoustica* 2002; **88**:463–471.

[25] Moureau V, Lartigue G, Sommerer Y, Angelberger C, Colin O, Poinsot T. Numerical methods for unsteady compressible multi-component reacting flows on fixed and moving grids. *Journal of Computational Physics* 2005; **202**(2):710–736.

FIGURES

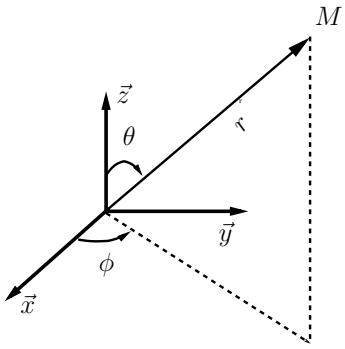

Figure 1. Spherical coordinates.

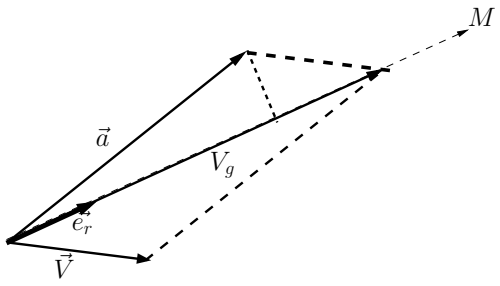

Figure 2. Group velocity of acoustic waves V_g.

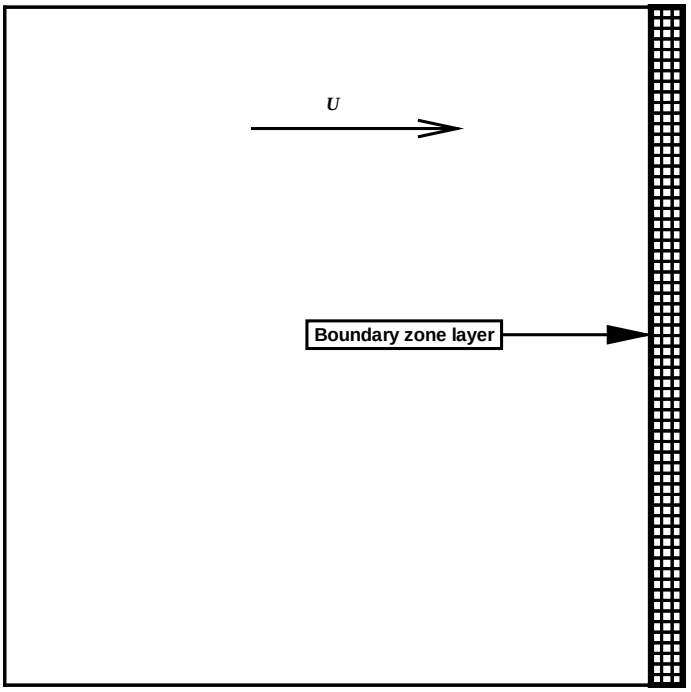

Figure 3. Tam and Dong outflow condition layer.

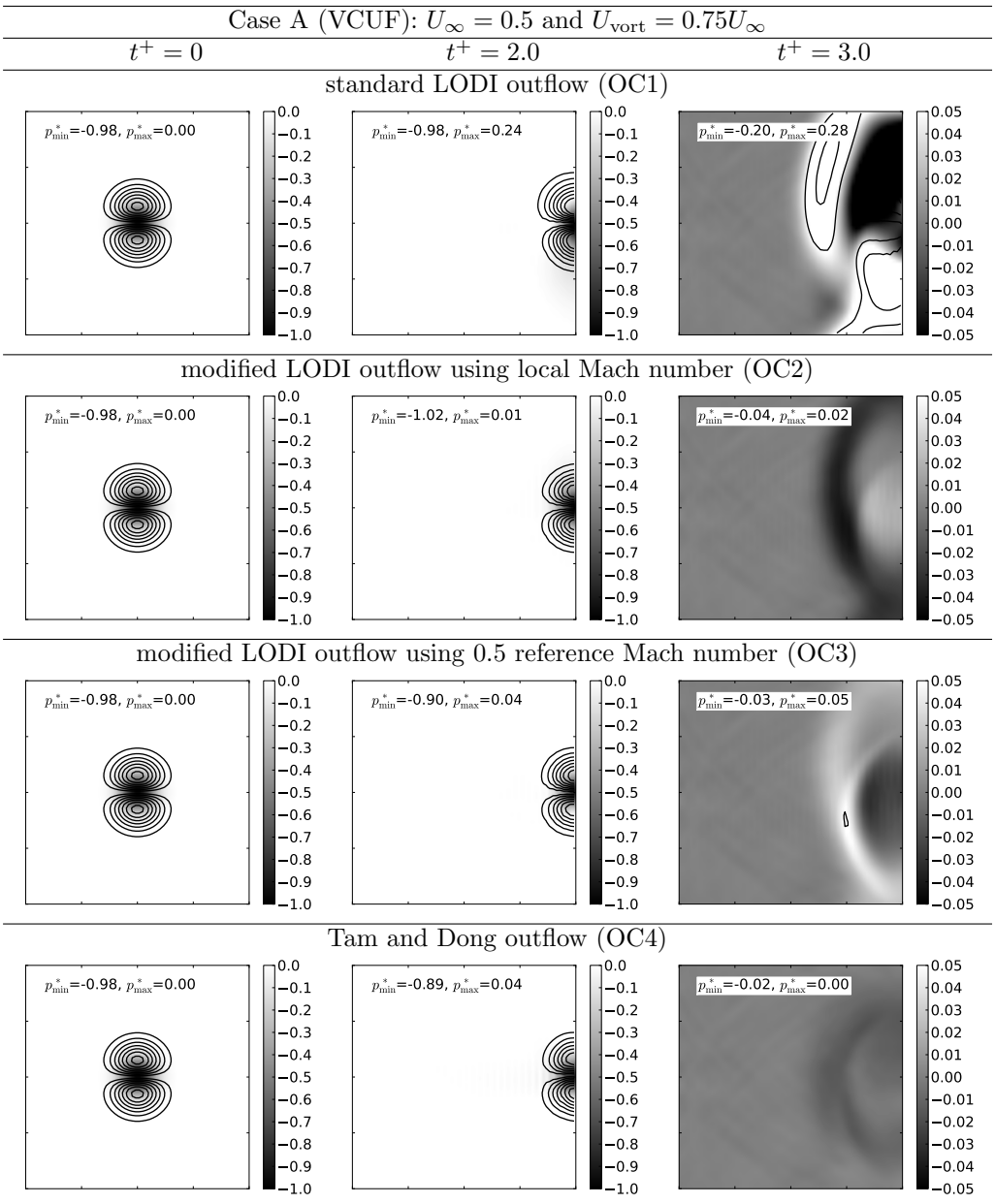

Figure 4. VCUF case A: streamwise velocity isocontours and normalized pressure grey scales.

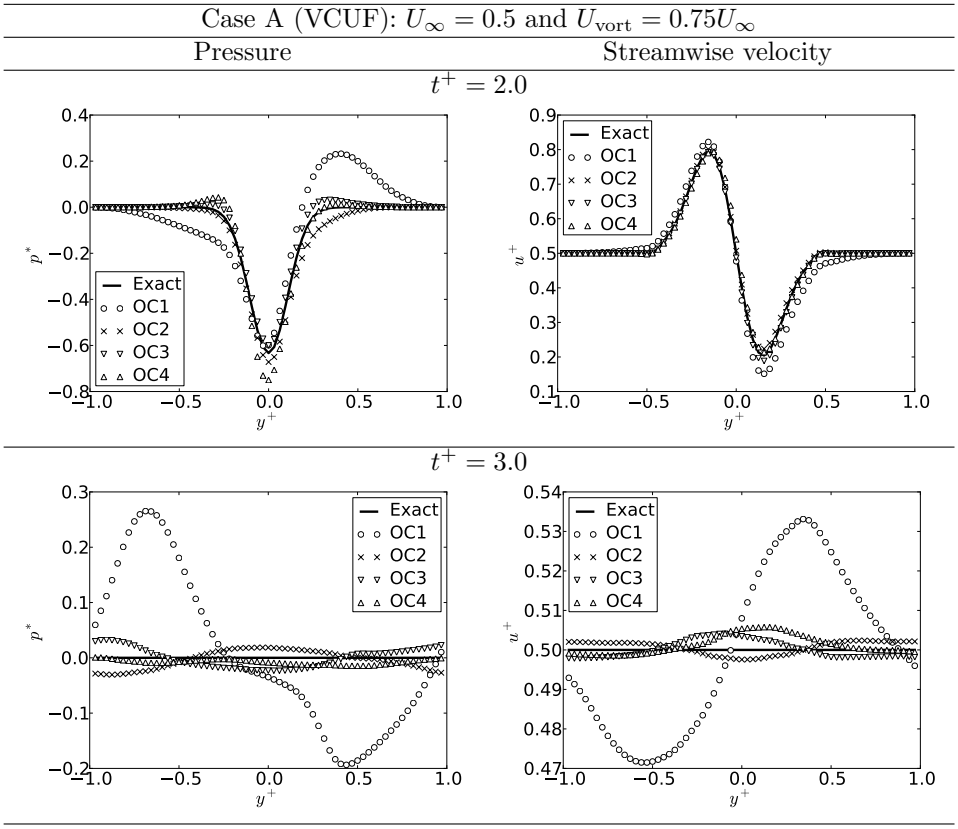

Figure 5. VCUF case A: profiles of the normalized pressure and streamwise velocity fields at $x = 0.9$.

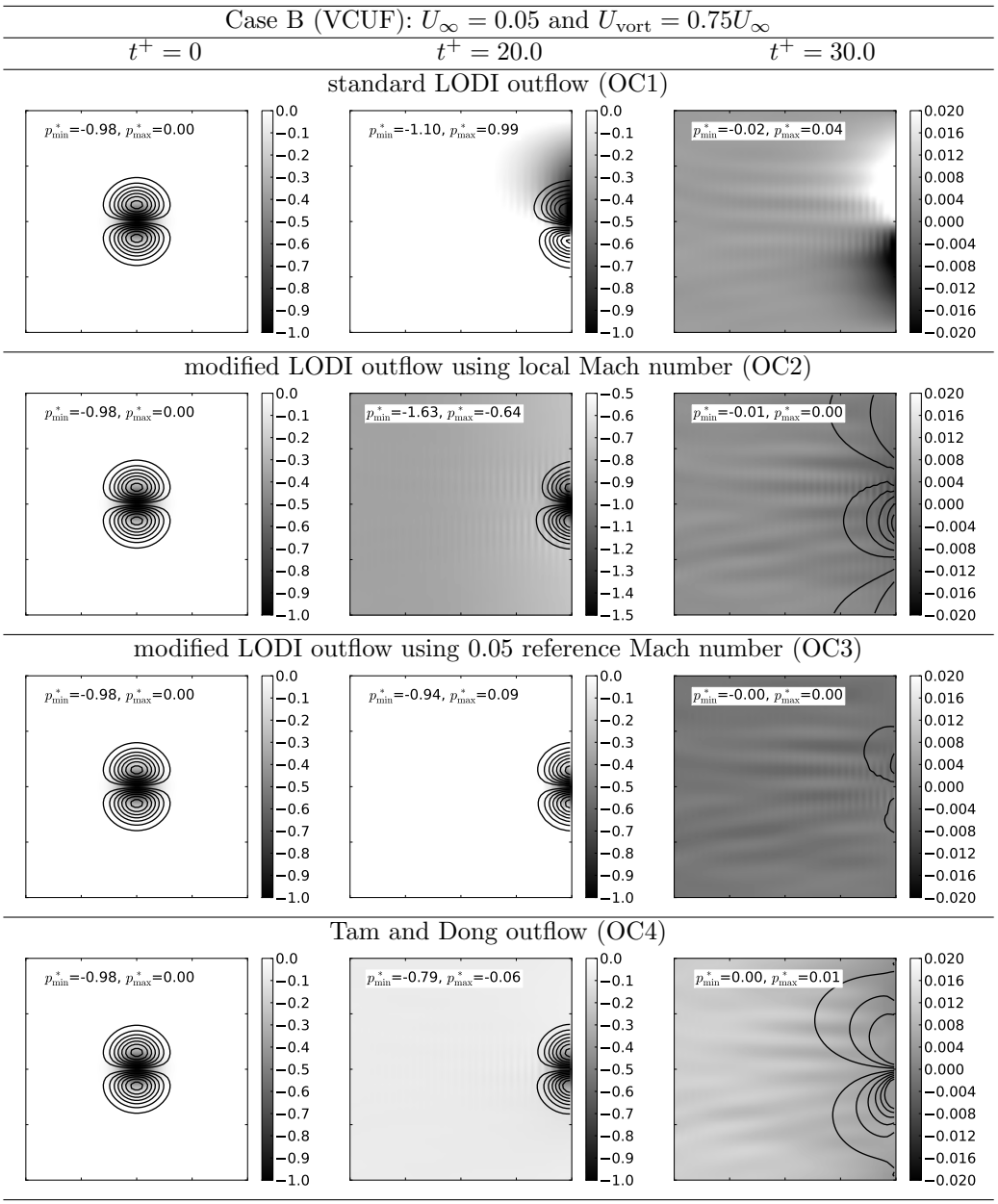

Figure 6. VCUF case B: streamwise velocity isocontours and normalized pressure grey scales.

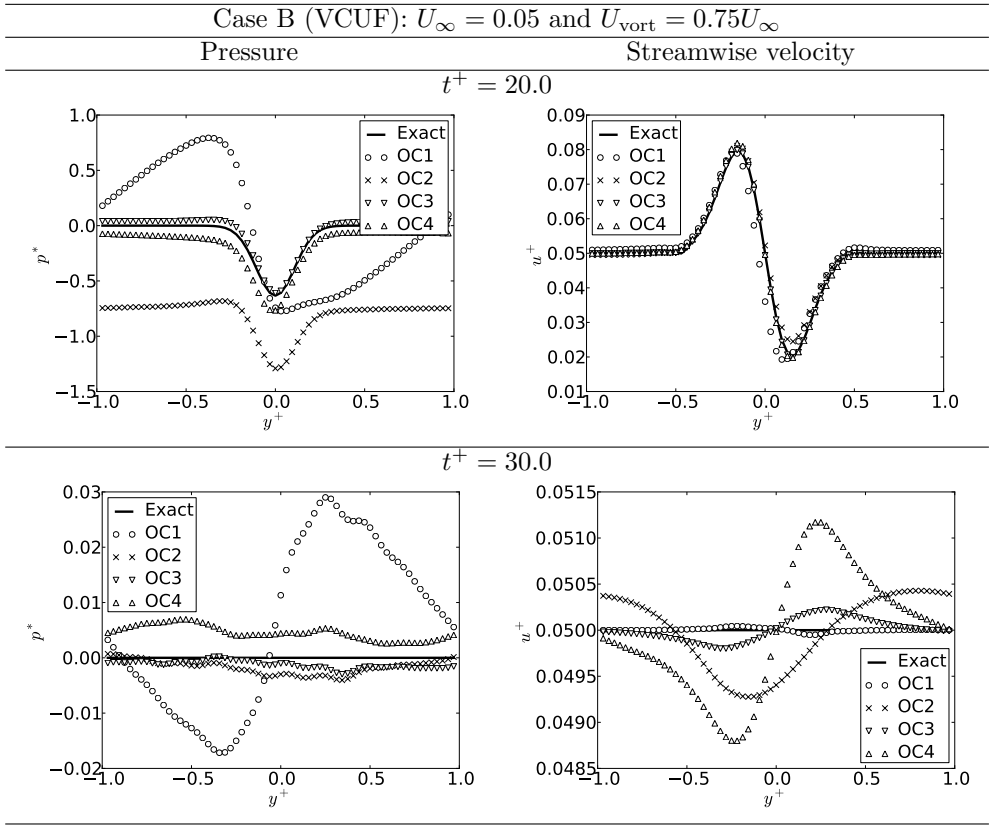

Figure 7. VCUF case B: profiles of the normalized pressure and streamwise velocity fields at $x = 0.9$.

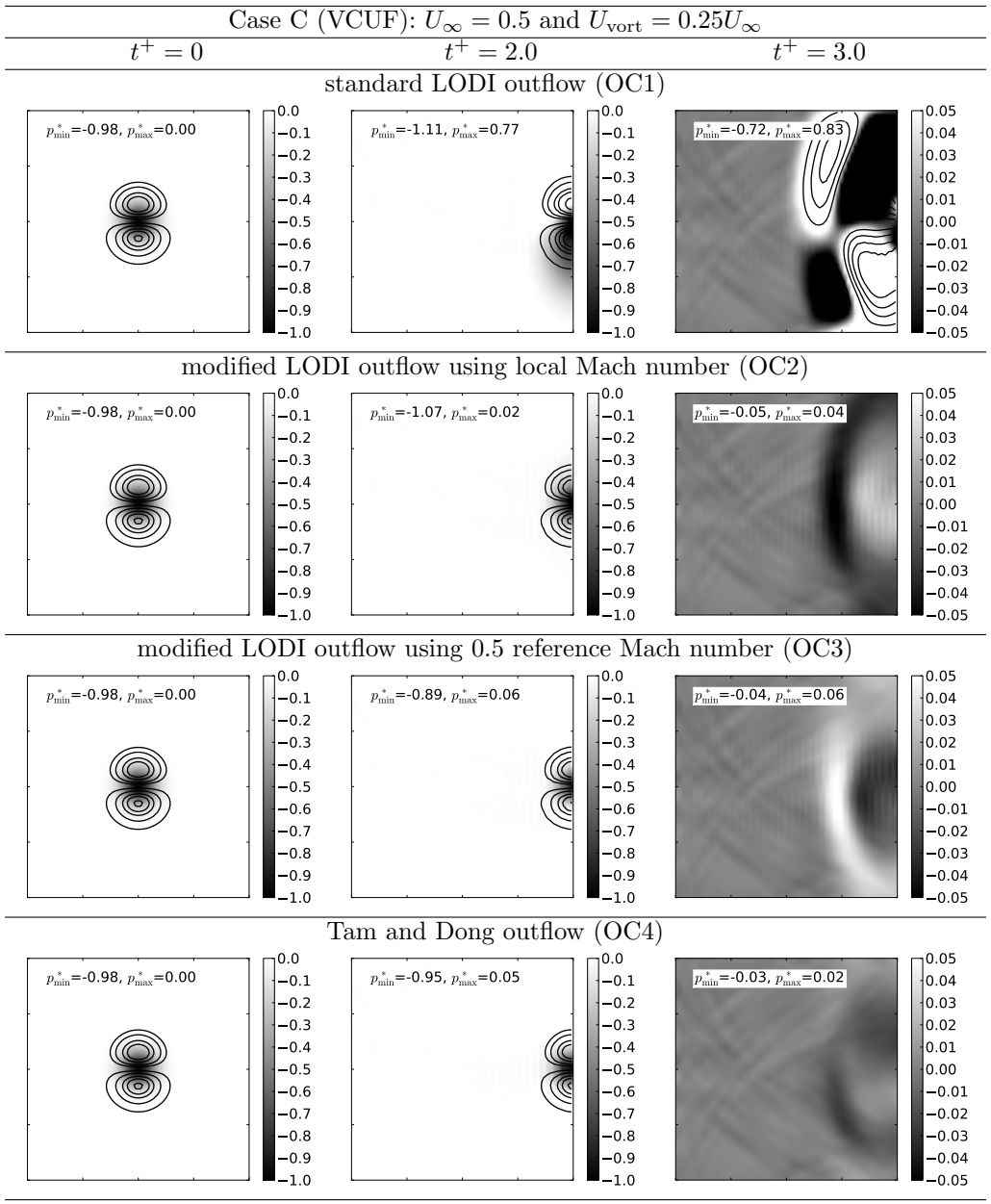

Figure 8. VCUF case C: streamwise velocity isocontours and normalized pressure grey scales.

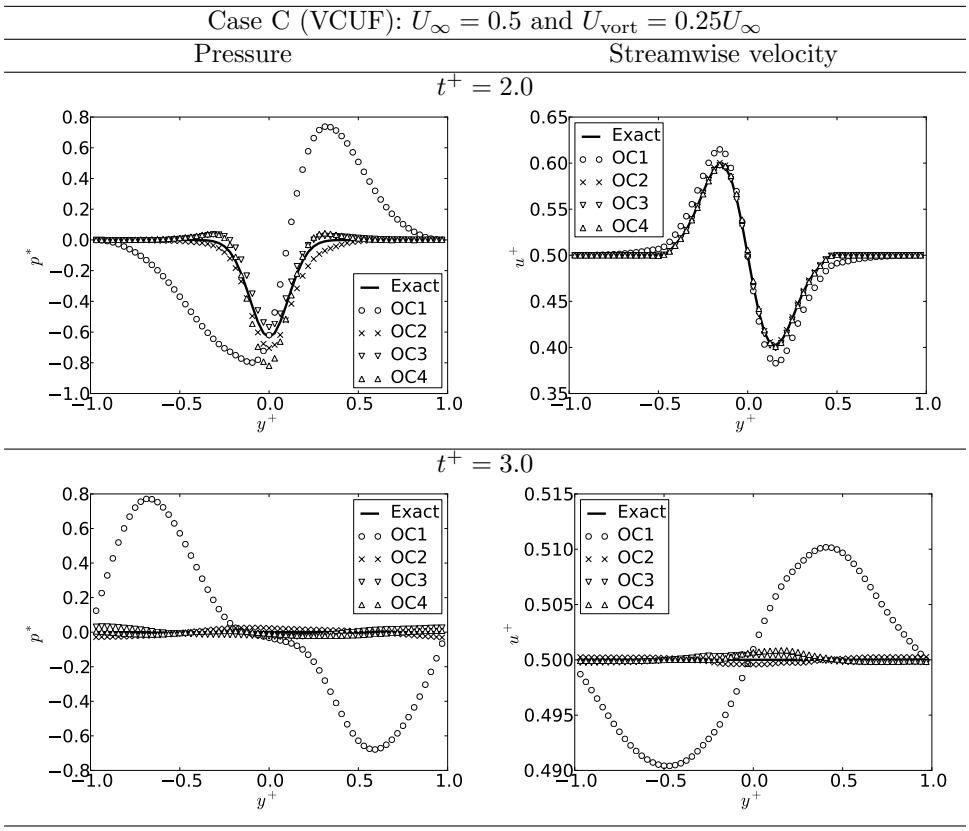

Figure 9. VCUF case C: profiles of the normalized pressure and streamwise velocity fields at $x = 0.9$.

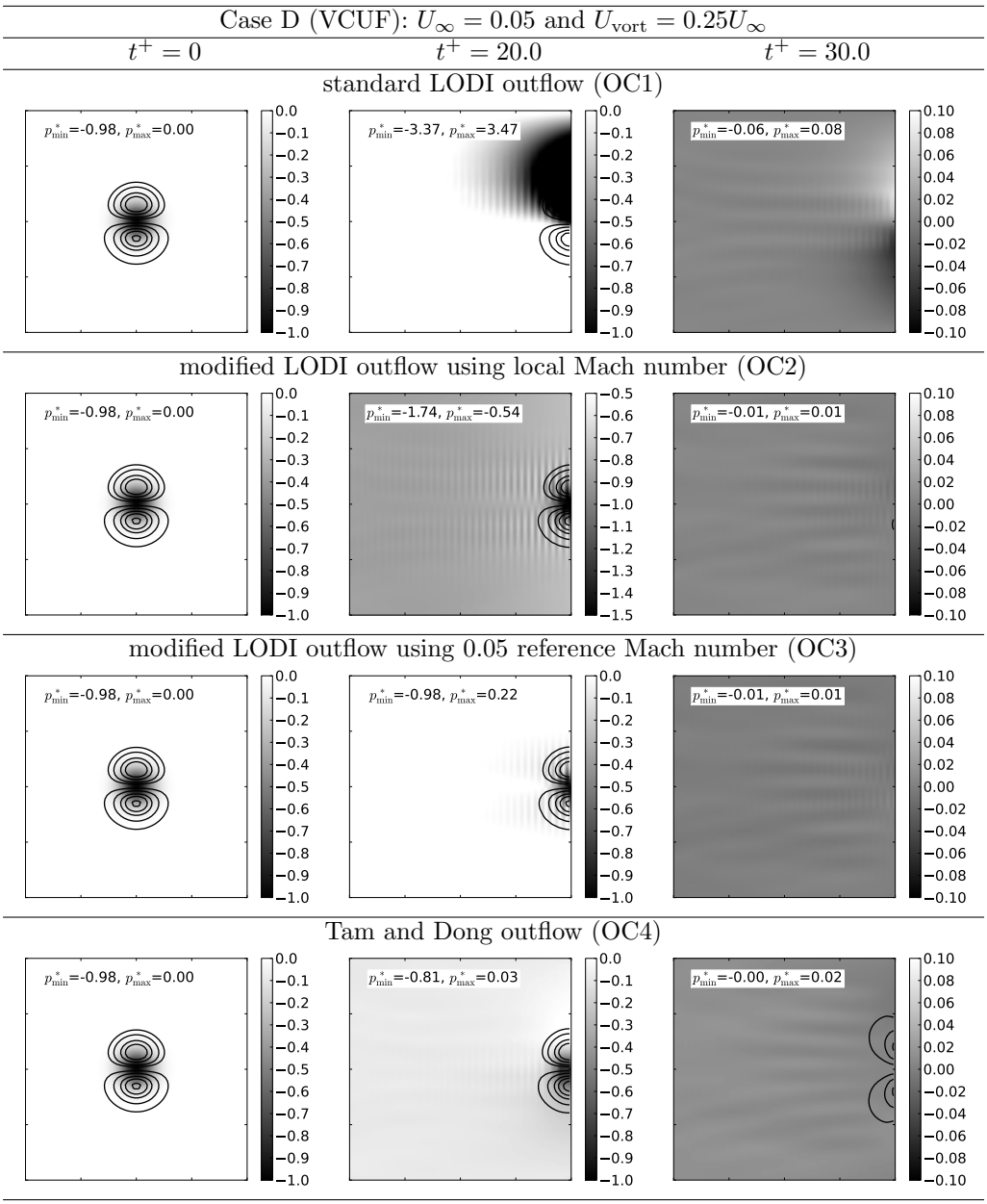

Figure 10. VCUF case D: streamwise velocity isocontours and normalized pressure grey scales.

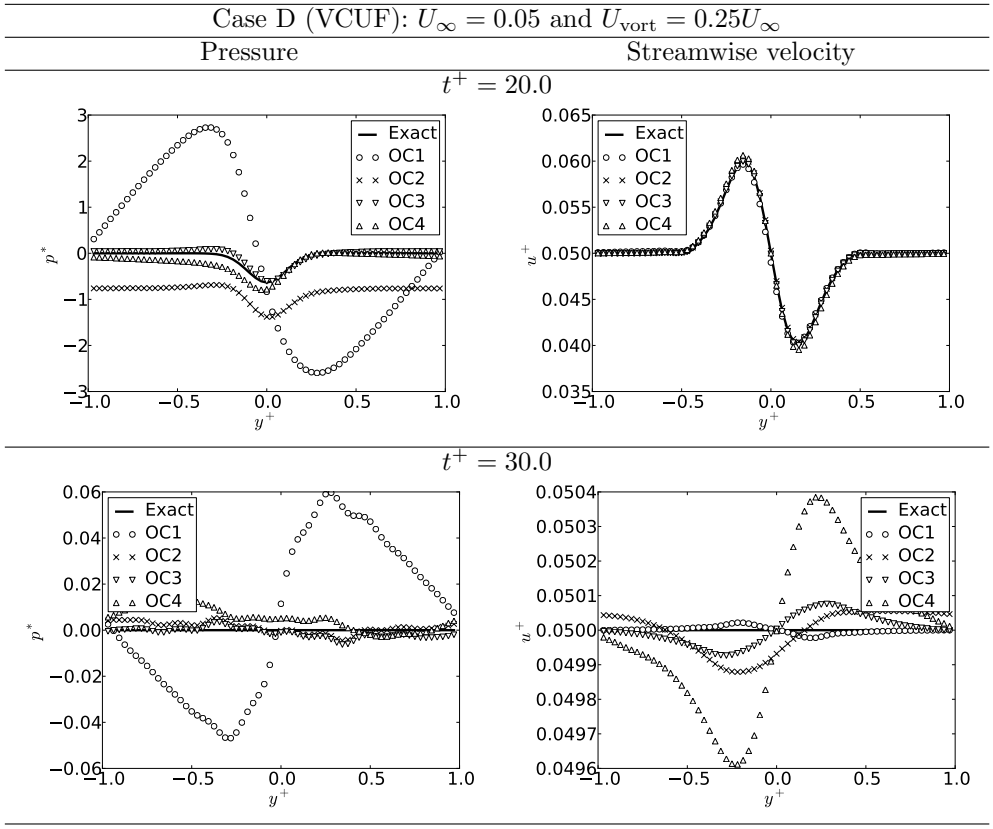

Figure 11. VCUF case D: profiles of the normalized pressure and streamwise velocity fields at $x = 0.9$.

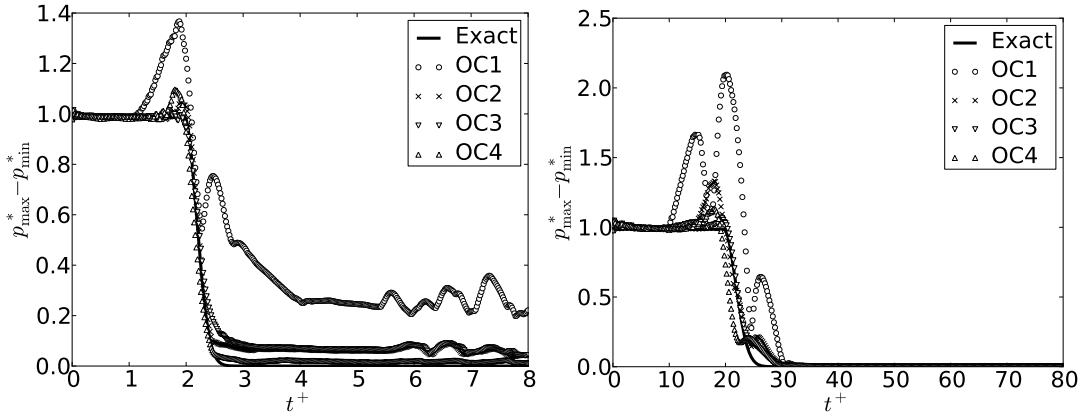

(a) case A

(b) case B

(c) case C

(d) case D

Figure 12. VCUF test problem: time evolution of $p^*_{\max} - p^*_{\min}$

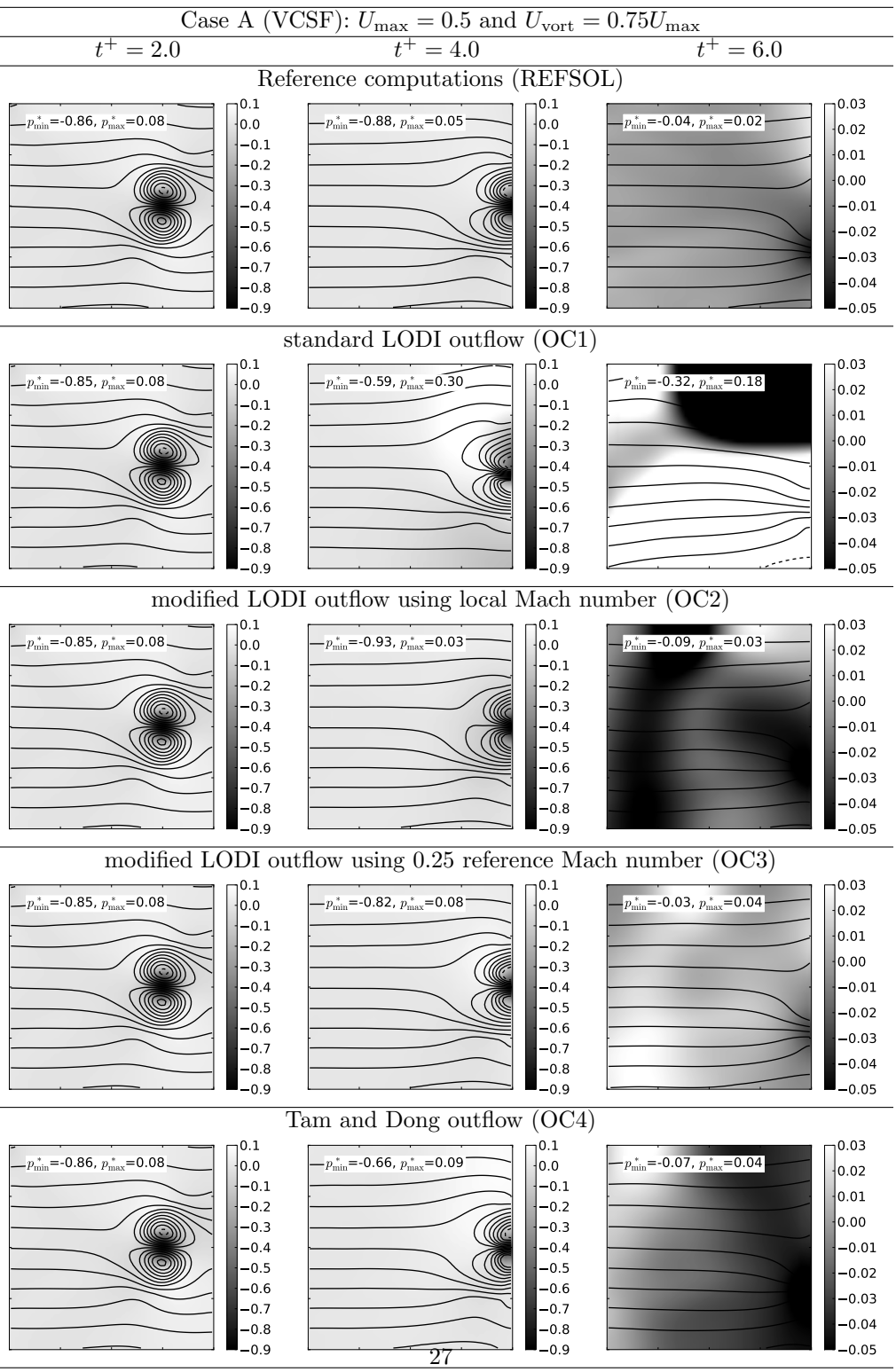

Figure 13. VCSF case A: streamwise velocity isocontours and normalized pressure grey scales.

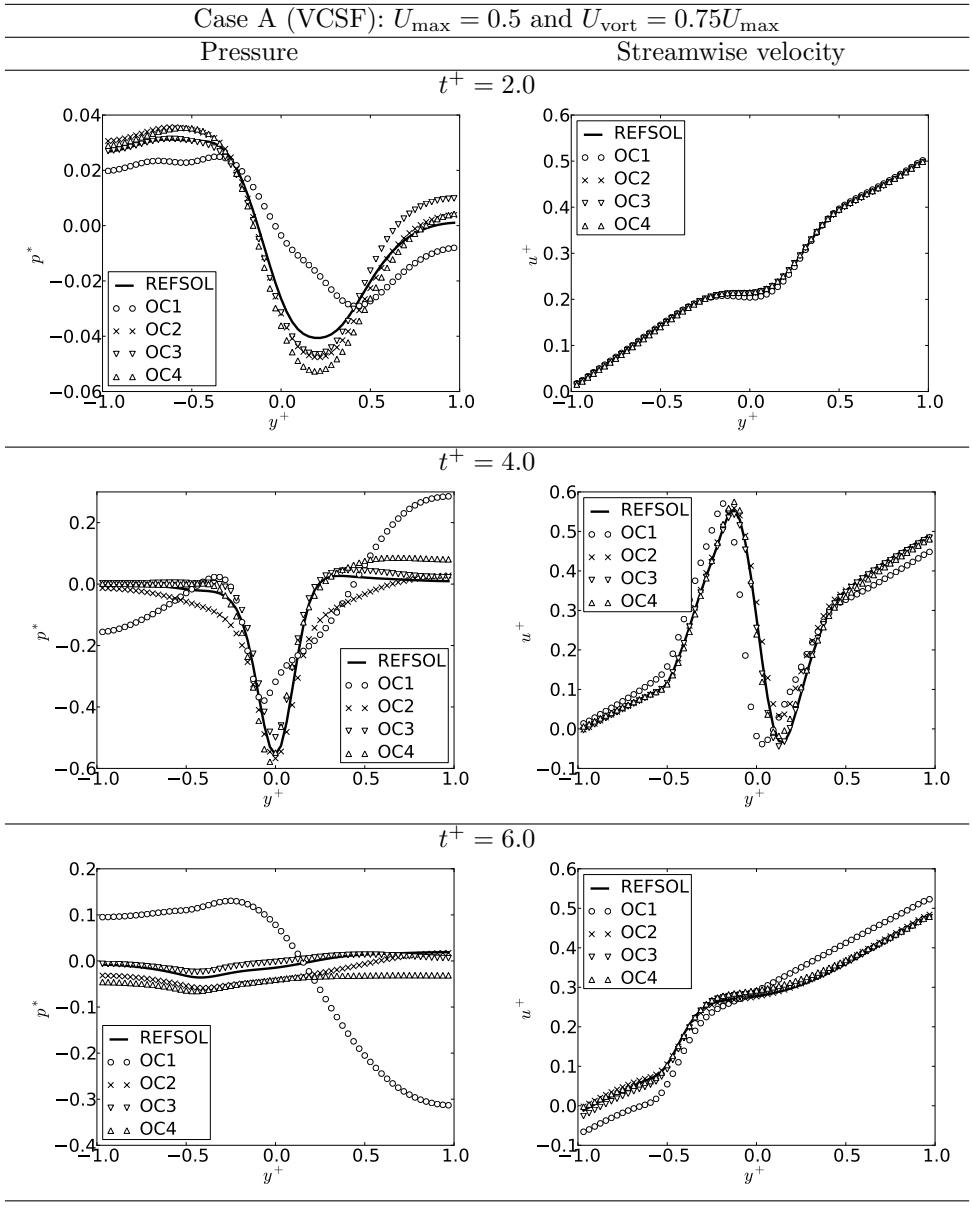

Figure 14. VCSF case A: profiles of the normalized pressure and streamwise velocity fields at $x = 0.9$ for different times.

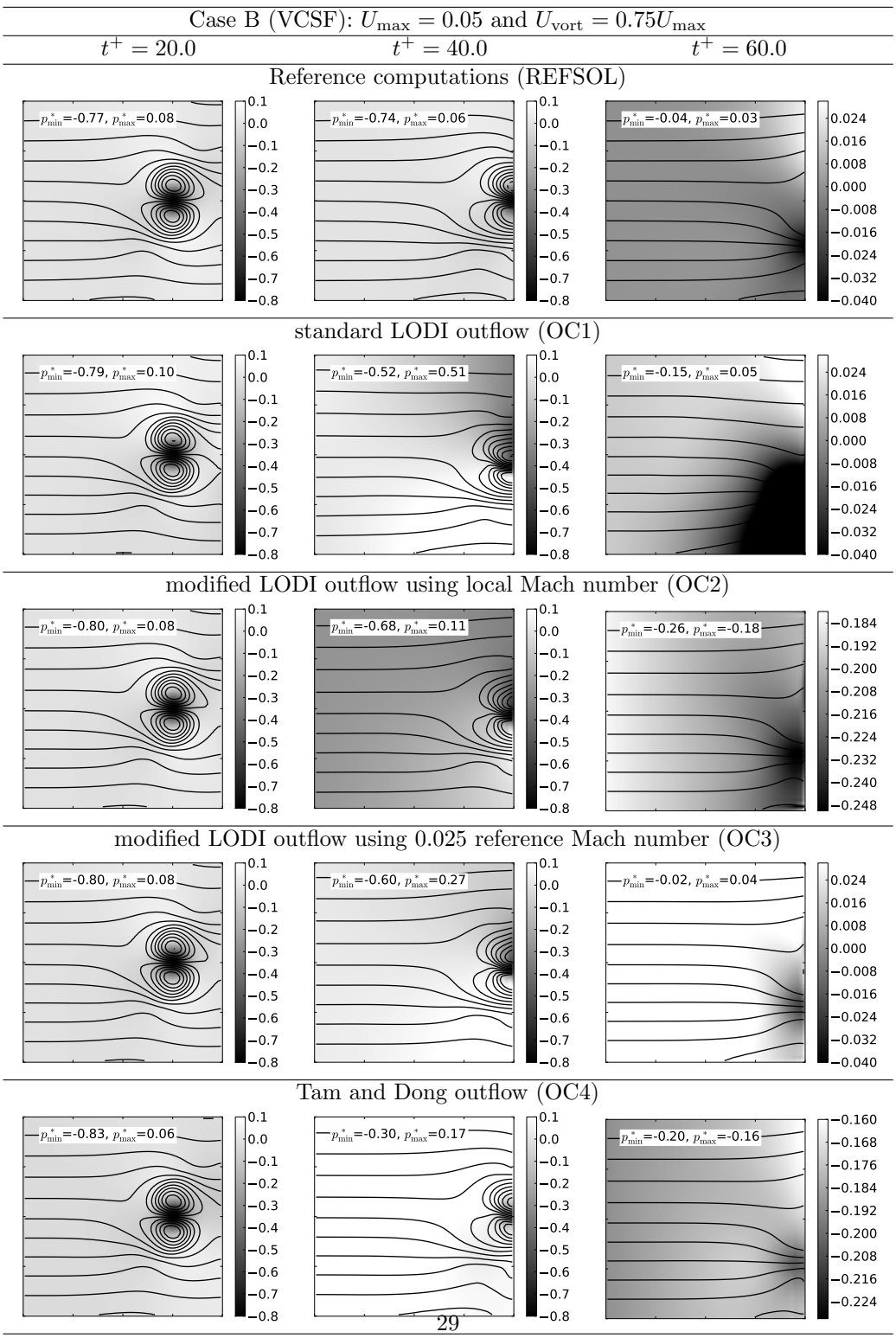

Figure 15. VCSF case B: streamwise velocity isocontours and normalized pressure grey scales.

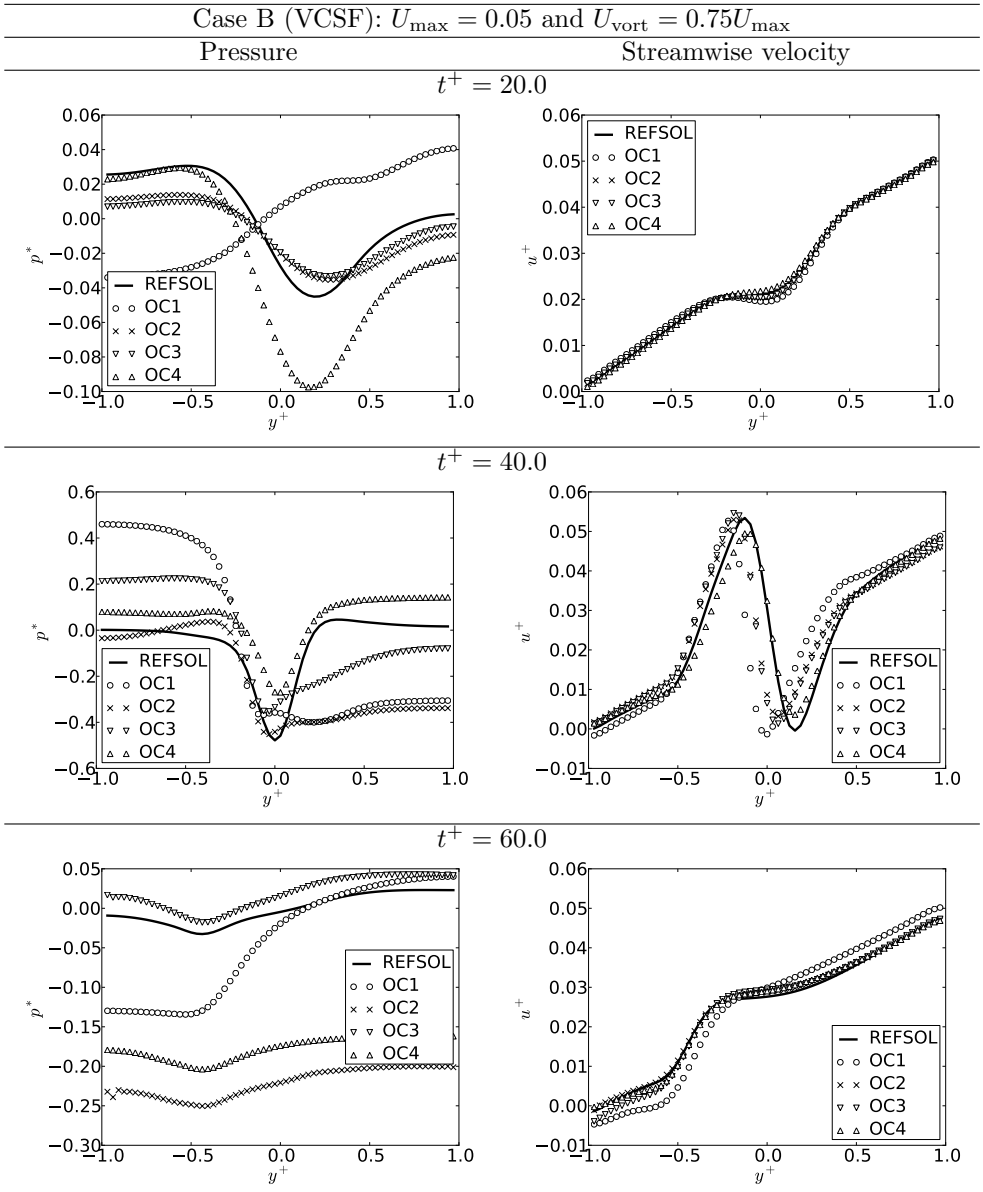

Figure 16. VCSF case B: profiles of the normalized pressure and streamwise velocity fields at $x = 0.9$ for different times.

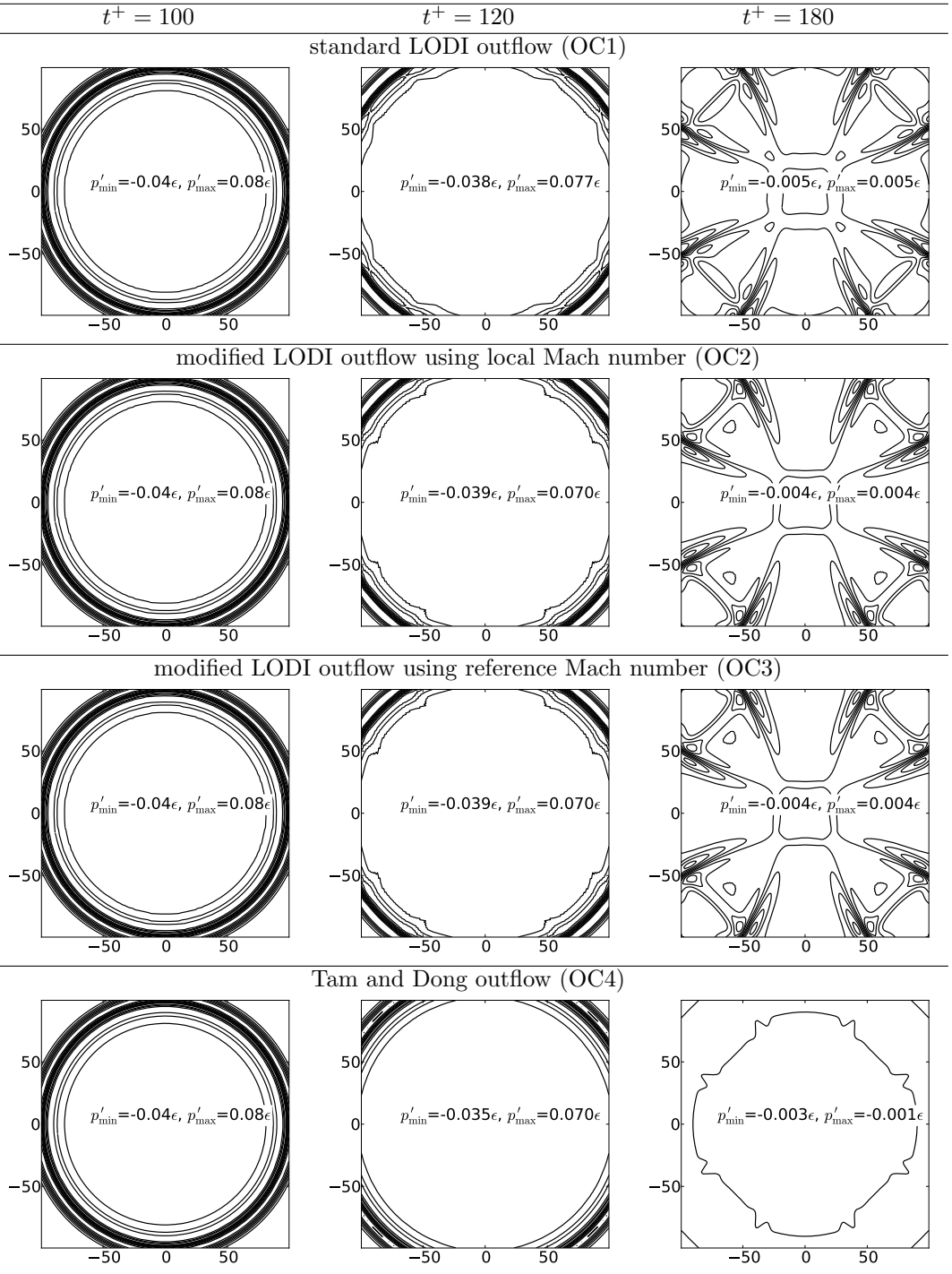

Figure 17. APM test problem: pressure isocontours at different times.

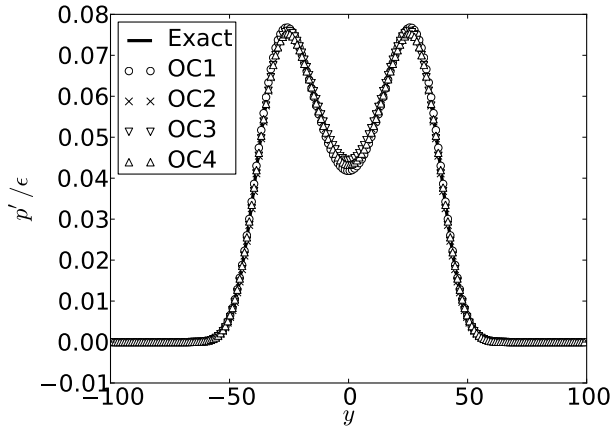

(a) $t^+ = 100$

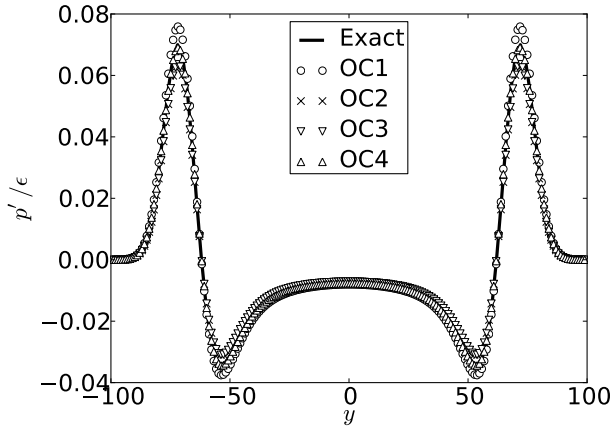

(b) $t^+ = 120$

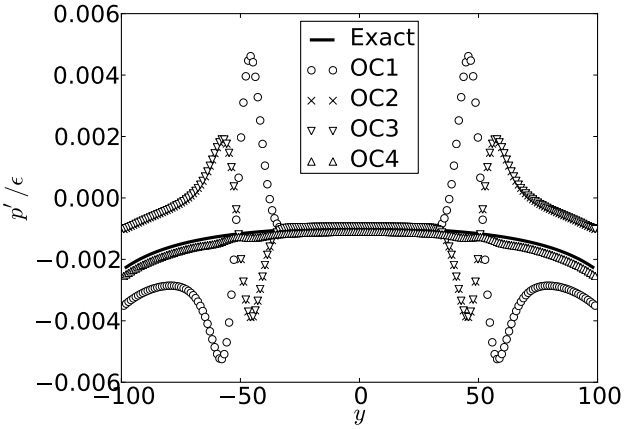

(c) $t^+ = 180$

Figure 18. Pressure profiles along the line $x = 99$ at different times for the propagation of an acoustic pulse (APM).

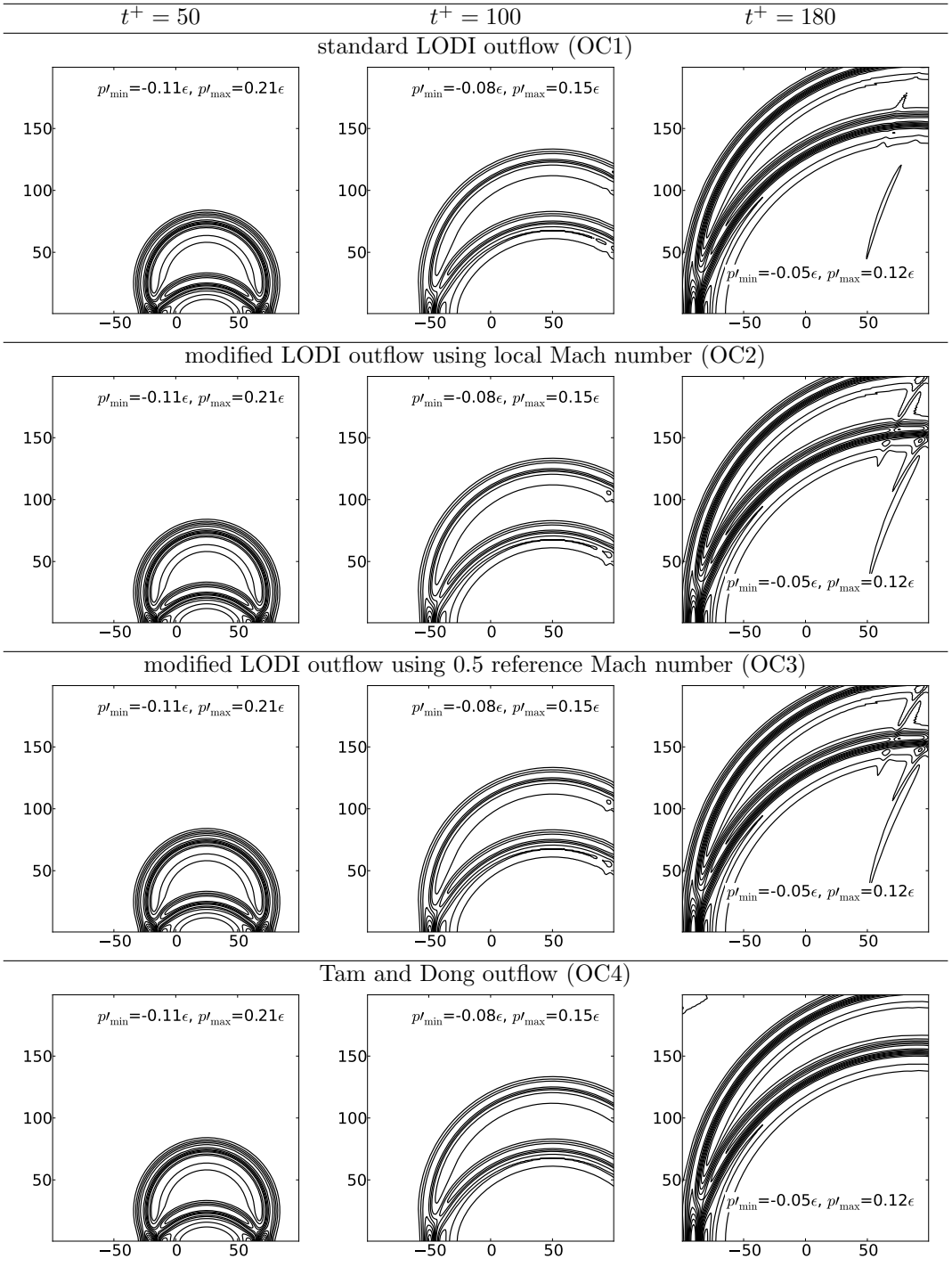

Figure 19. Pressure isocontours for the acoustic scattering by a plane test problem (APD).

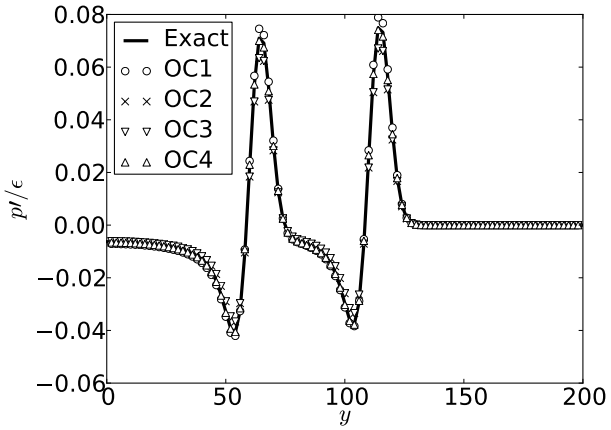

(a) $t^+ = 100$

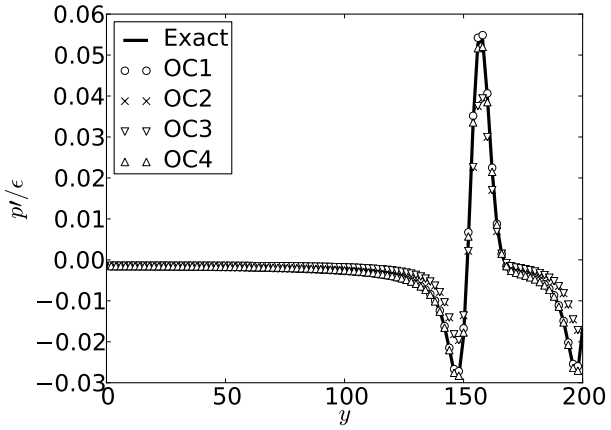

(b) $t^+ = 180$

Figure 20. Pressure profiles along the line $x = 99$ at different times for the acoustic scattering by a plane test (APD).